ACS Catalysis

Research Article

Cite This: ACS Catal. 2019, 9, 11371−11380

pubs.acs.org/acscatalysis

Robust and Versatile Host Protein for the Design and Evaluation of Artificial Metal Centers

Johannes Fischer,[†,‡,⊥,∇] Dominik Renn,[†,‡,∇] Felix Quitterer,[‡] Anand Radhakrishnan,[§,#] Meina Liu,[†] Arwa Makki,[†,¶] Seema Ghorpade,[†] Magnus Rueping,[†] Stefan T. Arold,*[,§,∥] Michael Groll,*[,‡] and Jörg Eppinger*[,†]

[†]KAUST Catalysis Center (KCC), Division of Physical Sciences & Engineering and [§]Computational Bioscience Research Center (CBRC), Division of Biological Sciences & Engineering, King Abdullah University of Science and Technology (KAUST), 23955 Thuwal, MK, Saudi Arabia

[‡]Center for Integrated Protein Science, Department Chemie, Lehrstuhl für Biochemie, Technische Universität München (TUM), D-85747 Garching, Germany

[∥]Centre de Biochimie Structurale, CNRS, INSERM, Université de Montpellier, 34090 Montpellier, France

Supporting Information

ABSTRACT: Artificial metalloenzymes (ArMs) have high potential in biotechnological applications as they combine the versatility of transition-metal catalysis with the substrate selectivity of enzymes. An ideal host protein should allow high-yield recombinant expression, display thermal and solvent stability to withstand harsh reaction conditions, lack nonspecific metal-binding residues, and contain a suitable cavity to accommodate the artificial metal site. Moreover, to allow its rational functionalization, the host should provide an intrinsic reporter for metal binding and structural changes, which should be readily amendable to high-resolution structural characterization. Herein, we present the design, characterization, and de novo functionalization of a fluorescent ArM scaffold, named mTFP*, that achieves these characteristics. Fluorescence measurements allowed direct assessment of the scaffold's structural integrity. Protein X-ray structures and transition metal Förster resonance energy transfer (tmFRET) studies validated the engineered metal coordination sites and provided insights into metal binding dynamics at the atomic level. The implemented active metal centers resulted in ArMs with efficient Diels−Alderase and Friedel−Crafts alkylase activities.

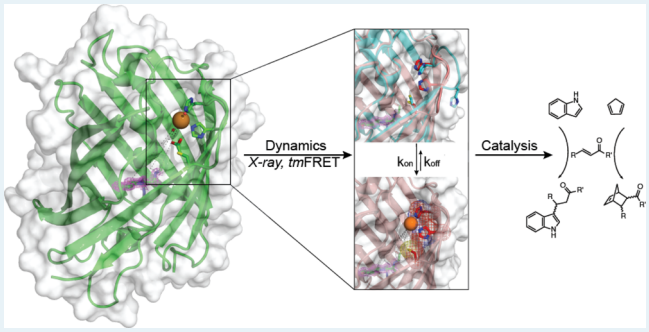

KEYWORDS: *artificial metalloenzyme, protein engineering, protein design, biocatalysis, metalloproteins, metalloenzyme, biohybrid catalysis*

1. INTRODUCTION

According to a recent estimate, more than half of all proteins are associated with metal ions in their active form.[1] It is, therefore, important to understand the factors that govern metal binding and reactivity in biological systems. Expanding the scope of nature's toolset through introduction of artificial metal centers and coordination geometries holds the promise to provide new techniques for chemical synthesis,[2−8] biocatalysis,[9−11] and biological research.[6,12−19] Various methods to generate artificial metalloenzymes (ArMs) were reported. These methods include domain-based directed evolution strategies[12,13,20−24] and strategies for engineering transition-metal binding sites by implementing (metal-chelating) unnatural amino acids[25−28] or by replacing the active site metal ions in naturally occurring metalloenzymes.[28−30] Other approaches use covalent[31−47] or supramolecular insertion of metal-containing artificial cofactors.[48−53] Some systems achieve impressive efficiencies and enantioselectivities[53−55] or benefit from coactivation through the second coordination sphere within a protein specificity pocket.[56,57] However, when compared to molecular catalysts, ArMs suffer from low stability toward elevated temperatures, pH changes, and/or solubility in organic solvents. Additionally, their synthesis and catalytic activity typically require specific chemical modifications or ligands. These limitations preclude simple recombinant production and complicate in vivo applications. To attenuate these limitations, several groups developed various techniques[58−60] to enhance the efficacy and applicability of ArMs, in particular based on computational methods[61−65] and large-scale (high-throughput) screening.[53,66−70] For instance, an artificial copper binding site was incorporated inside the central cavity of the thermophilic TIM-

Received: July 9, 2019
Revised: October 16, 2019

DOI: 10.1021/acscatal.9b02896
ACS Catal. 2019, 9, 11371−11380

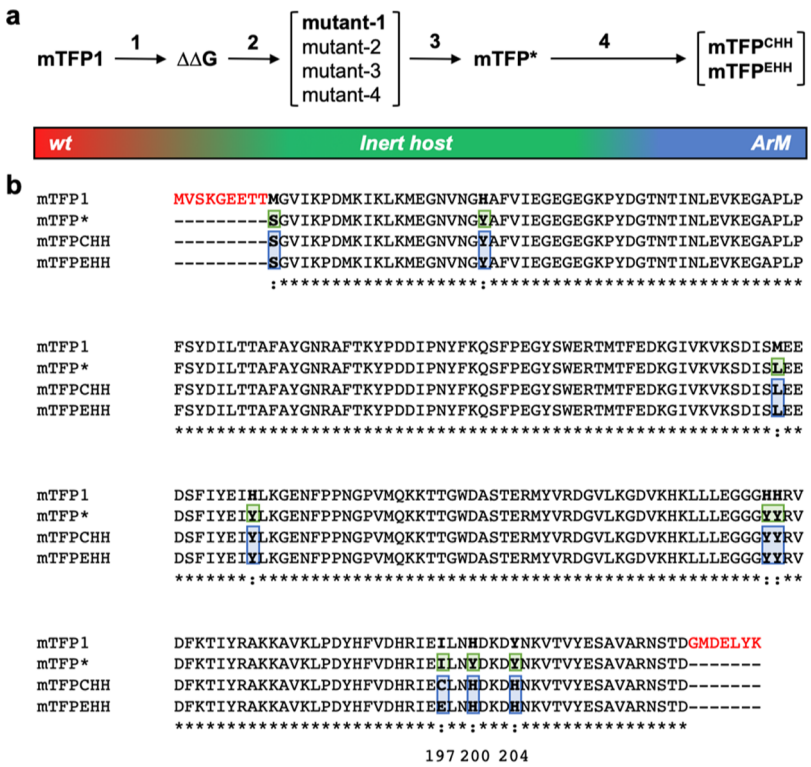

Figure 1. (a) Strategy used: starting from mTFP1, in silico designed point mutations were ranked according to their calculated stability (1), then assessed in silico for thermal stability (2), the resulting constructs were experimentally tested (3), yielding the stable and inert mTFP*, and scaffold functionalization was used to derive metal binding ArMs (4). (b) Mutations associated with the different design steps: residues in red have been removed, bold residues indicate mutation sites, where green indicates positions to achieve the inert host, and blue achieves the rationally designed ArMs.

barrel glycerol phosphate synthase *Thermotoga maritima*, tHisF, through mutational analysis.[71] This strategy of engineering metal binding sites from canonical amino acids is highly appealing as the generation of a suitable metal coordinating geometry only requires conventional site-specific mutagenesis, eliminating complicated synthesis, bioconjugation, and purification steps to add ligands and cofactors. In parallel, other groups advanced the individual steps required to produce a catalytically active ArM based on canonical amino acids, namely, (i) engineering the affinity and selectivity of metal binding toward peptides[72−76] and proteins,[18,58,77,78] (ii) elucidating the three-dimensional architectures of metal coordination by proteins,[7,79−82] and (iii) altering the catalytic activity of the existing metalloproteins.[18,83,84] Nevertheless, it remains challenging to introduce de novo metal binding sites, based on canonical amino acids, to allow functionalization of an inert scaffold for catalytical chemistry applications.[67,71,85−88]

In particular, one of the remaining difficulties in the design of such an ArM is to predict its affinity and selectivity for different metals.[56,67] Hence, it is uncertain under which conditions a potential (natural or engineered) metal binding site coordinates with metal ions and to what extent this site is selective. A host protein should therefore have a reporter mechanism, which allows direct observation of metal binding and changes in protein structure. Also, to facilitate quantification of metal coordination, the host should display a least amount of (nonspecific) metal binding residues on its surface and comprise a cavity to accommodate the artificial metal site. Additionally, the ArM protein needs to express well, be purified easily, and show a high stability toward temperature, pH, and organic solvents.

Intrinsic protein fluorescence can be used to determine the metal binding properties if the introduced metal association modifies the protein's fluorescence features. This principle was adopted to introduce transition metal ion Förster resonance energy transfer (tmFRET).[89,90] Given a sufficient spectral overlap, the light emission of the chromophore of fluorescent proteins is quenched when a transition metal is coordinated at a distance less than the Förster radius.[91] Thus, the fluorescence alterations predominantly result from resonant energy transfer between the metal ion and the chromophore, whereas static quenching, electron transfer, or perturbation of the protein's structure typically results in only minor changes.[8,85,86] Moreover, dynamic collision quenching (described by a Stern−Volmer constant K_{SV}) becomes important at high metal concentrations. Because the tmFRET intensity depends on the occupation of the binding site, the metal−chromophore distance, and the spectral overlap of fluorophore emission and metal absorption bands, tmFRET data can quantify protein−metal affinities and provide insights into the nature of the binding event.

We demonstrate the design, characterization, and application of a novel fluorescent ArM scaffold, named mTFP*. The intrinsic fluorescence of this exceptionally stable host allowed fast quantification of metal binding thermodynamics and revealed subtle changes in coordination geometries for different mutants. Additionally, mTFP* crystallizes easily and therefore facilitates rational design of metal binding pockets based on high-resolution X-ray structures. Because mTFP* was engineered to minimize background metal ion binding, it presents an attractive system to introduce novel metal binding sites. We further prove the suitability of the mTFP* scaffold as

DOI: 10.1021/acscatal.9b02896
ACS Catal. 2019, 9, 11371−11380

a versatile template for rationally designed biocatalysts through producing the mTFP*-derived artificial copper enzymes $mTFP^{CHH}$ and $mTFP^{EHH}$, which have Friedel–Crafts alkylase[92−95] and Diels–Alderase activity.[96−100]

2. ENGINEERING THE HOST PROTEIN mTFP*

To identify an ArM host protein that allows quantification of metal binding through the tmFRET concept,[89,90] we investigated highly stable fluorescent proteins. Based on the available literature data, structural information and homology modeling,[101,102] we chose mTFP1[103] as a parent scaffold. mTFP1 is a monomeric, bright, and photostable version of the *Clavularia* cyan fluorescent protein that combines temperature and pH stability with a bright fluorescence (ε = 64 000 M^{-1} cm^{-1}, Φ = 64) and spectral characteristics applicable for tmFRET (absorbance: 462 nm, emission: 492 nm).[103] Moreover, mTFP1 can be produced recombinantly in large amounts, which exhibits a cavity with dimensions similar to catalytic centers of natural metalloenzymes.[104] Hence, the pocket's second coordination sphere can interact with a substrate bound to the metal center and thus might control substrate orientation and coactivation.

Incorporating catalytically active late transition metals, which are not available to nature, is a particular motivation in ArM design.[8] However, such metals preferentially coordinate with intermediate or soft Lewis bases. These nonspecific interactions compete with engineered binding sites and therefore complicate ArM development. Thus, hosts for de novo design should be depleted of surface-exposed His, Met, and Cys. Accordingly, we replaced in silico six surface-exposed amino acid side chains (H30Y, M118L, H128Y, H177Y, H178Y, and H209Y) within mTFP1 (PDB: 2HQK).[103] Analysis of the hydrogen-bonding networks and evolutionary conservation indicated structural tolerance of these mutations (see the Supporting Note and Table S1). In order to select substitutions that do not reduce the stability of mTFP1, we performed an in silico design strategy (Figure 1a).

We used FoldX[105,106] to computationally evaluate the stability of 30 mTFP1 mutants (Table S2) and submitted the four best scorings to molecular dynamics (MD) simulations (Table S3 and Supporting Note). Although all of these mutants did not display increased thermal mobility (Figures 2a, S1), we noted that the N- and C-terminal sequences (MVSKEETTM and GMDELYK, respectively) (Table S4) of mTFP1 showed high flexibility in simulations in agreement that they are not resolved in the X-ray structure (PDB: 2HQK).[103] Thus, both short sequences were removed to avoid unwanted interference or potential metal coordination. After the successful completion of molecular cloning and protein expression of these candidates, mutant-1 revealed the highest purification yields [500 mg of protein per liter culture of BL21 (DE3) gold cells] and was accordingly selected as our host protein scaffold, which we named mTFP* (Figure S2).

3. mTFP* SCAFFOLD IS HIGHLY STABLE AND CAN ACT AS A FLUORESCENT REPORTER

mTFP* had an absorbance maximum at 468 nm and a fluorescent emission peak at 495 nm (Figure S3a). In comparison to mTFP1, these values are red-shifted by about 3 nm. Because the emission signal of the chromophore serves as an intrinsic probe to estimate the amount of correctly folded mTFP* protein in solution,[107] the stability of mTFP*-derived artificial (metallo)proteins can easily be determined using standardized fluorescence and absorbance measurements.

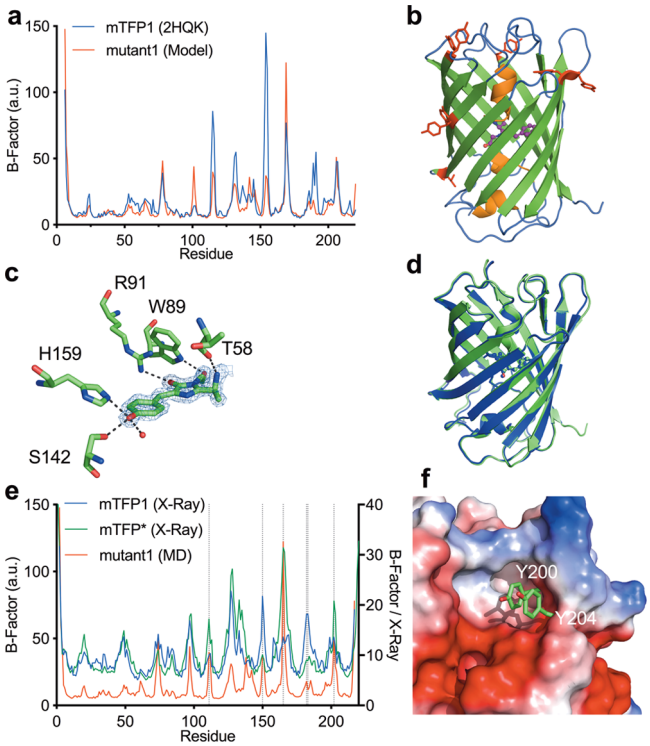

Figure 2. (a) Comparison of B-factors obtained after 50 ns of MD simulation for mTFP1 (based on the PDB 2HKQ[103] as a starting model) and for mutant1 (named mTFP* hereafter). (b) Crystal structure of mTFP* at 1.00 Å resolution. The antiparallel sheet is represented in green, connecting loops in blue, and the α-helix in orange. The chromophore is shown as balls and sticks (purple). Modified residues are highlighted in red. (c) Chromophore of mTFP* with coordinating residues T58, W89, R91, S142, and H159. The $2F_o-F_e$ electron density map of the chromophore is shown in blue and contoured at 1σ. (d) Structural superposition of mTFP1 (blue) and mTFP* (green) match onto each other with a root-mean-square deviation (rmsd) of C^α atoms <0.2 Å. (e) B-Factor comparison of mutants representing the overall low thermal mobility and structural integrity, as indicated by dashed lines. (f) Surface representation of the catalytic cavity in mTFP* (PDB: 4Q9W). Surface colors indicate positive and negative potentials contoured from 20 kT/e (intense blue) and −20 kT/e (intense red). Residues Y200 and Y204, used to build the coordination site, are shown.

Notably, mTFP* displayed a marked decrease in circular dichroism ellipticity at 205 nm between 87 and 90 °C (Figure S3b,c). At 80 °C, the addition of chaotropic reagents such as urea (10 M) did not decrease the fluorescence signal over a time period of 30 min (Figure S4a,b). At 25 °C, circular dichroism and fluorescence data indicated that the structural integrity of mTFP* is preserved within a pH range from 2.3 to 12.6 (Figure S4c). Moreover, the protein is soluble up to concentrations of 2 mM in buffer and can withstand high concentrations of organic solvents (Figure S4d,e).

Next, we determined the X-ray structure of mTFP* to a resolution of 1.0 Å (R_{Free} = 15.0%; PDB: 4Q9W). The coordinates of mTFP1 (PDB: 2HQK)[103] acted as a template to perform Patterson search calculations using the software PHASER.[108] The well-defined electron density map depicted the entire mTFP* protein (Table S5). The monomer adopts a β-barrel fold composed of 11 antiparallel β-sheets around the

DOI: 10.1021/acscatal.9b02896
ACS Catal. 2019, 9, 11371−11380

central A62−Y63−G64 chromophore (Figure 2b), which is stabilized by the H-bonding network including residues T58, W89, R91, S142, and H159 (Figure 2c). None of the six mutations we introduced in mTFP* caused significant structural perturbations relative to mTFP1 (Figure 2d). However, as predicted by the MD simulations, B-factor comparison revealed that the neighboring loops D150−G151 and K180−Y188 in mTFP* are conformationally constrained, while the mobility of the loops surrounding the cleft between sheets 7, 8, and 10 (L163−G167 and Y-200−Y204) is markedly increased (Figure 2e). This higher flexibility is favorable for ArMs, as we will show below, by allowing the mutated residues within the cleft to rearrange during metal binding.

4. mTFP* DISPLAYS A MARGINAL BACKGROUND AFFINITY TO TRANSITION-METAL IONS

To assess unspecific metal binding affinity of mTFP*, we incubated 0.2 mM mTFP* with Cu^{2+}, Ni^{2+}, Rh^{3+}, and Pd^{2+} ions (sulfates or nitrates) for up to 24 h (Figure S5a,b) and attempted to revert quenching through dialysis (Figure 3).

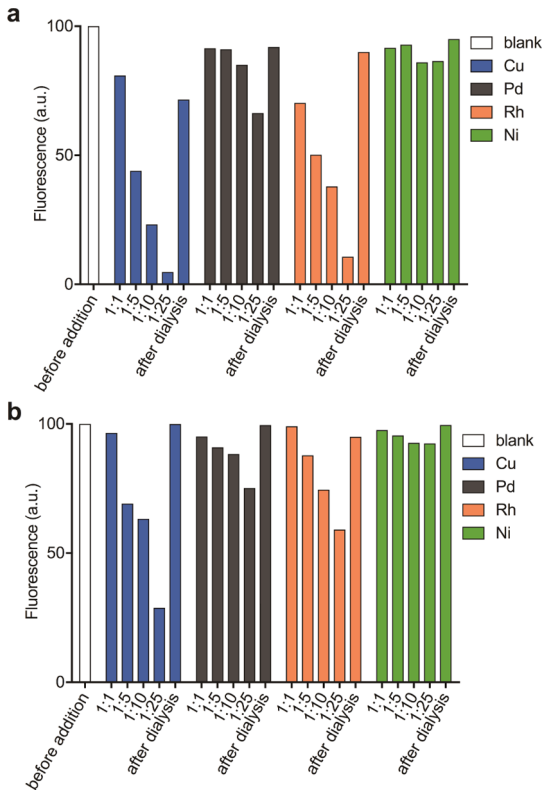

Figure 3. (a,b) Fluorescence measurement of mTFP1 (a) and mTFP* (b). The samples were soaked in 1, 5, 10, and 25 equiv of Cu^{2+}, Pd^{2+}, Rh^{2+}, and Ni^{2+}, respectively, for 24 h. Binding reversibilities were confirmed throughout signal recovery after dialysis. Note that the quenching efficiency depends on the specific spectral overlap between metal and protein.

Metal binding below 25 equiv of Cu^{2+}, Rh^{3+}, or Pd^{2+} ions was neither detected by electrospray ionization mass spectrometry (ESI-MS) nor by matrix-assisted laser desorption/ionization-time-of-flight MS (MALDI-TOF MS). At high equivalents (1:5 and above), a correlated decrease of mTFP* fluorescence indicated the emergence of a tmFRET signal (Figures 3a,b, S5, and Table S6). Ultimately, the fluorescence of mTFP* was fully restored after dialysis, demonstrating that metal coordination was weak and reversible (Figure 3a,b). Soaking experiments carried out for 10 min further confirmed these observations (Figure S5). Conversely, the tmFRET quenching effect was markedly enhanced for mTFP1, which persisted after dialysis (Figure 3).

To determine the binding affinity of mTFP* to Cu^{2+}, we performed tmFRET titration experiments (Figure 4a,b and

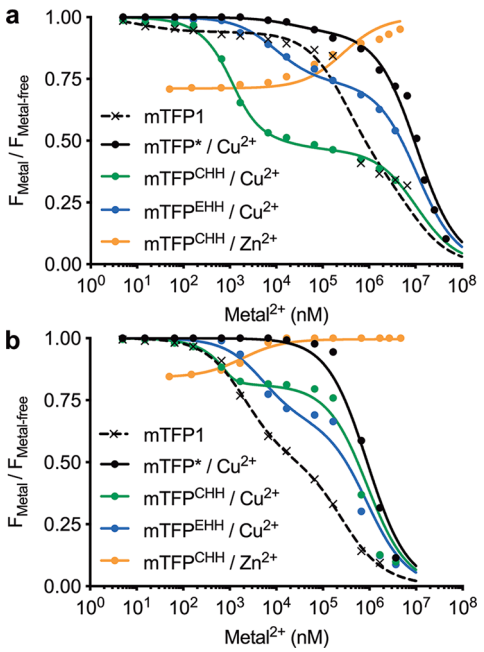

Figure 4. (a) Metal coordination at pH 6.0 indicates copper and zinc binding for $mTFP^{CHH}$ and $mTFP^{EHH}$ along with the ancestor mTFP1. No metal binding occurred in the mTFP* scaffold. (b) Metal coordination at pH 7.5 reveals copper and zinc binding for $mTFP^{CHH}$ and $mTFP^{EHH}$, whereas no metal binding was measured for the mTFP* scaffold.

Supporting Note—tmFRET). At the high metal concentrations used in these experiments (up to 0.1 mM), dynamic collision quenching becomes important, which can be described by a Stern−Volmer constant K_{SV}. Curve fitting to a single-site binding model (Supporting Note) revealed dynamic quenching at high Cu^{2+} concentrations with a K_{SV} of 0.09 ± 0.01 mM^{-1} at pH = 6 and 1.12 ± 0.14 mM^{-1} at pH = 7.5 (Table S7). Conversely, tmFRET data of mTFP1 required at least two specific binding constants K_d^{site} of 0.02 ± 0.01 μM and K_d^{back} 330 ± 151 μM (pH = 6) or 2.14 ± 0.29 and 268 ± 125 μM (pH = 7.5) to achieve a satisfying curve fit (R > 0.95) (Table S7), revealing additional nonspecific binding events for mTFP1, but not for mTFP*.

5. INTRODUCING SPECIFIC TRANSITION-METAL BINDING SITES INTO mTFP*

Our X-ray structures revealed that residues from β-sheets 7, 8, 10, 11, and the central helix constitute a cavity that is about 1.1 nm wide, 1.3 nm deep, and 1.7 nm long. These dimensions are typical for catalytic centers of metal enzymes.[104] Moreover, the distance between the chromophore and the cleft (1.05−2.30 nm) is within the appropriate range for tmFRET studies.[109] Therefore, we chose this cavity for our engineering approach. Residue Y200 sits in the center of this cavity (Figure 2f).

DOI: 10.1021/acscatal.9b02896
ACS Catal. 2019, 9, 11371−11380

Because this position corresponds to H209 in mTFP1 (Figure 1b, Table S4), we chose mutation Y200H as our starting point to engineer an artificial metal binding site. By inspecting the homology model of this mutant, we identified positions D54, Y55, I197, and Y204 as potential sites for the introduction of additional metal binding His, Glu, or Cys residues. An in silico point mutation analysis by FoldX predicted the mutants I197C−Y200H−Y204H ($mTFP^{CHH}$) and I197E−Y200H−Y204H ($mTFP^{EHH}$) as the most stable variants. These changes were introduced using site-directed mutagenesis (Figure 1b), and the heterologous protein expression yielded >200 mg/L of highly pure protein (Figure S2) with spectroscopic characteristics and heat/pH stabilities similar to those of mTFP* (Figure S6).

$mTFP^{CHH}$ and $mTFP^{EHH}$ crystalized under conditions similar to those established for mTFP* at pH = 7.5 (Table S5, $mTFP^{CHH}$: R_{Free} = 18.4%; PDB: 6QSL; $mTFP^{EHH}$: R_{Free} = 19.8; PDB: 6QSO). In both X-ray structures, the side chains of the introduced metal chelating amino acids point toward the inside of the cavity (Figure 5a,b).

Conversely, $mTFP^{CHH}$ crystals grown from acidic conditions (pH = 6.0) revealed a second conformation (Table S5, R_{Free} = 19.6%; PDB: 6QSM), in which residue H200 was turned outward to reduce the repulsive columbic interaction of the two positively charged side chains H200 and H204 (Figure 5c). In the following, we refer to the pH 6.0 conformation as "open" and pH 7.5 structures as "closed". This "open" conformation underlined the flexibility of residues 197−206 of β-strand 10 (Figure 5e,f) which was stabilized by a hydrogen bond between the protonated H200 and T208. This structural rearrangement reduced the distance between C197 and H204 from 5.7 to 5.2 Å. Next, we determined the crystal structure of $mTFP^{CHH}$ with a 1:1.1 excess of $CuSO_4$ at pH = 7.5 (Table S5, R_{Free} = 19.4%; PDB: 4R6D). This structure closely resembled mTFP* with a root-mean-square deviation (RMSD) of 1.1 Å and one Cu^{2+} ion in the center of the protein cleft, 1.5 nm away from the AYG_{62-64} chromophore (Figure S7a). For both H200 and H204, the short N−Cu^{2+} distances of 2.1 Å indicated a dative bonding interaction between the metal atom center and the two histidine side chains. The Cu^{2+} coordination, which is completed by two water molecules, reduced the thermal flexibility of the residues 195−210 (Figures 5e and S6b) and caused a minor rearrangement of the flexible part of strand 10, enhancing the Cu−S distance to 5.7 Å. Therefore, the Cu^{2+} coordination only involved H200 and H204 (Figure 5d), contrary to our force field-based calculations which suggested an implication of C197.

To verify the metal coordination of those crystal forms for which we did not obtain copper complex structures (open $mTFP^{CHH}$ and closed $mTFP^{EHH}$), we used their respective apo structures to establish the models of these complexes (Figure S7b,c). In these crystal structures, C197 and H204 ($mTFP^{CHH}$/open), as well as E197, H200, and H204 ($mTFP^{EHH}$), revealed a promising preorientation for metal binding [$d(S_{C197}-N_{H204})$ = 5.2 Å; $d(O_{E197}-N_{H200})$ = 4.6 Å, $d(O_{C197}-N_{H204})$ = 3.0 Å, and $d(N_{H200}-N_{H204})$ = 3.7Å] (Figure 5a,b). In silico introduction of a copper center induced only minor rearrangements of these residues during energy minimization. Thus, our X-ray data and in silico analysis confirmed that Cu^{2+} coordination is possible for all forms, whereby $mTFP^{CHH}$ involves either residues H200 and H204 (closed form) or C197 and H204 (open form). Conversely, the copper binding motif of the mutant $mTFP^{EHH}$ involves all three residues E197, H200, and H204 (Figure 5a−d).

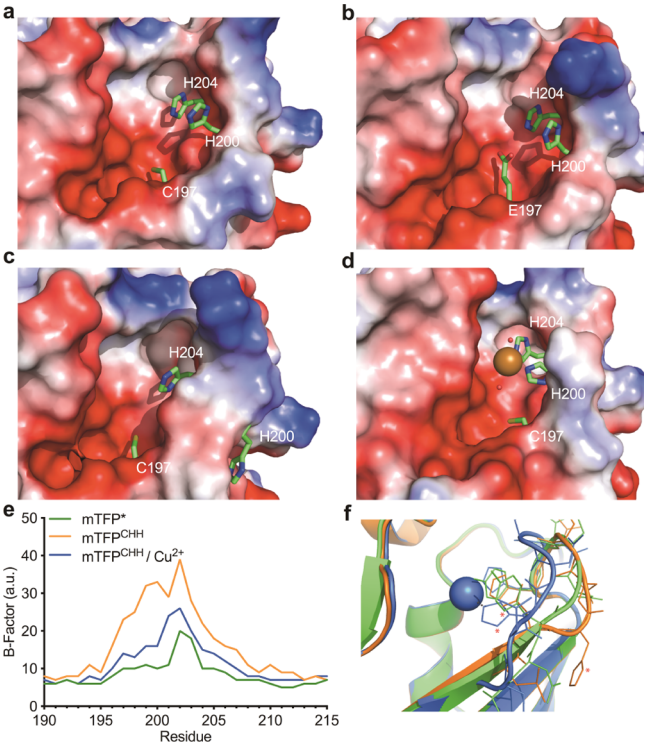

Figure 5. (a−d) Crystal structures of the catalytic clefts of $mTFP^{CHH}$ (closed configuration) at pH 7.5 (a), $mTFP^{EHH}$ (b), $mTFP^{CHH}$ (open configuration) at pH 6.0 (c) with open configuration undergoing structural rearrangement in the course of pH change (a,c), and cocrystallized structure of $mTFP^{CHH}$ coordinating a Cu^{2+} ion (d). Surface colors indicate positive and negative electrostatic potentials contoured from 20 kT/e (blue) and −20 kT/e (red). The coordination residues are represented in sticks (a−d). (e) B-factor comparison of mTFP*, $mTFP^{CHH}$, and $mTFP^{CHH}/Cu^{2+}$ indicating a stabilized coordination throughout the copper coordination by His−His-motive. (f) Superposition mTFP*(green), $mTFP^{CHH}$ (orange), and Cu^{2+}−$mTFP^{CHH}$, visualizing the structural rearrangements of the cleft flanking loop, especially upon Cu^{2+} ion coordination (* indicates the shift of residue Y/H200).

6. tmFRET ASSAYS REVEALED METAL COORDINATION AND pH-DEPENDENT REARRANGEMENTS

In agreement with our structural data, fluorescence measurements via tmFRET revealed a stable metal coordination in $mTFP^{CHH}$ and $mTFP^{EHH}$ at both pH 6.0 and 7.5. Curve fitting of tmFRET experiments (Figure 4) allowed us to determine the apparent K_d^{site} values of Cu^{2+} for $mTFP^{CHH}$ to be 0.56 ± 0.06 μM at pH 6.0 and 0.05 ± 0.01 μM at pH 7.5, whereas for $mTFP^{EHH}$, they were 8.2 ± 1.5 μM at pH 6.0 and 4.5 ± 2.7 μM at pH 7.5 (Table S7).

The signals indicated a 1:1 complex of the $mTFP^{CHH}$ or $mTFP^{EHH}$ mutant protein and Cu^{2+}, which was verified by liquid chromatography (LC)−ESI−MS and inductively coupled plasma (ICP)-MS data (Figure S8, Tables S6 and S8). Conversely, these methods did not show Cu^{2+} coordination by mTFP* (Tables S6 and S8). The metal binding to both artificial sites proved to be highly stable, preserving a metal atom occupancy above 50% following 24 h of dialysis in buffer without metal ions (Figure S5c). In

DOI: 10.1021/acscatal.9b02896
ACS Catal. 2019, 9, 11371−11380

addition, fluorescence quenching was observed after 24 h of dialysis for other transition-metal ions, which increased in the order Ni^{2+} < Rh^{3+} < Pd^{2+} < Cu^{2+} for $mTFP^{CHH}$ (with a fluorescence recovery of 99, 81, 85, and 67%, respectively), indicating that $mTFP^{CHH}$ can also coordinate with other transition metals than copper. As expected, the fluorescent recovery was close to 100% for mTFP* for all these metals (Figure S5, Supporting Note—tmFRET).

Titrations of copper-loaded $mTFP^{CHH}$ or $mTFP^{EHH}$ in the presence of Zn^{2+} fully restored the fluorescence of the apo protein, with affinities of 128 ± 32 μM at pH 6.0 and 4.01 ± 0.14 μM at pH 7.5, while $mTFP^{EHH}$ titrations resulted in 288 ± 118 μM at pH 7.5 (Figure 4, Table S7). Thus, through competition experiments with copper-loaded mTFP* variants, tmFRET can be used to study the binding process of transition metals, for which the spectral overlap integral is negligible.

7. ARTIFICIAL CU−PROTEINS ARE CATALYTICALLY ACTIVE AND ACHIEVE HIGH STEREOINDUCTION

To evaluate the potential catalysis of our artificial Cu−proteins, we conducted [4 + 2] cycloadditions, commonly known as Diels−Alder reactions (Figure 6a, Table S9). The activity assays displayed a distinct pH profile for the copper-coordinated cysteine mutant Cu^{2+}−$mTFP^{CHH}$ (Figure 6b, Table S9), while the glutamate variant $mTFP^{EHH}$ delivered quantitative yields over a pH range from 3.5 to 7.5 with low enantioselectivities (Table S9). In the next series of experiments, we analyzed the Friedel−Crafts alkylation with our engineered $mTFP^{CHH}$ and $mTFP^{EHH}$ copper proteins. We measured excellent enantioselectivities in the reaction of α,β-unsaturated 2-acylimidazole with indole (Figure 6c, Table S9).

Notably, $mTFP^{CHH}$ produced stereoselectivities of up to 92% ee (Figure 6d, Table S9), while $mTFP^{EHH}$ achieved an ee between 40 and 93%. Background reactions without added $Cu(NO_3)_2$ showed no considerable conversions. In comparison, nonchelated Cu^{2+} ions achieved over 90% conversion, however, without enantio- or stereocontrol (Table S9, Supporting Note). The lower rate of the artificial enzyme may be due to (passive) steric restrictions.[110,111] For the Friedel−Crafts alkylation, the pH variation from 5.0 to 7.5 had only a minor impact on both the catalytic activity and the stereoinduction of $mTFP^{CHH}$ or $mTFP^{EHH}$, suggesting that the Cu^{2+} ion is firmly bound and shielded in the protein pocket.

Following this demonstration of basic catalytic functionality, we tested whether changes within the second coordination sphere would further enhance the Diels−Alder activity of the mutant, $mTFP^{CHH}$. From our X-ray analysis and additional MD simulations, we concluded that a smaller, more hydrophobic, and sterically restricted binding site would improve the substrate coordination. Moreover, the selectivity might increase and presumably cause a stronger coordination of the Diels−Alder substrate (Figure S9a). Consequently, we replaced residues at the edge of the cleft containing the metal binding motif with more polar and hydrophobic amino acids (K135A, T137S, E164G, G165K, I197Y, N199Y, D201K, and K202Y) (Figure S9a). The corresponding optimized $mTFP^{CHH}$ mutant, $mTFP^{CHH\ opti}$, showed catalytically enhanced stereoselectivities and accelerated reaction rates, for example, doubled for pH 6.0 (Figure S9). The most obvious increase was at pH 6.0, where the introduced mutations consistently accounted for a boost from 2 to 26% enantiomeric excess. Thus, catalysis of our ArM can be further enhanced through modifications of its second coordination sphere.

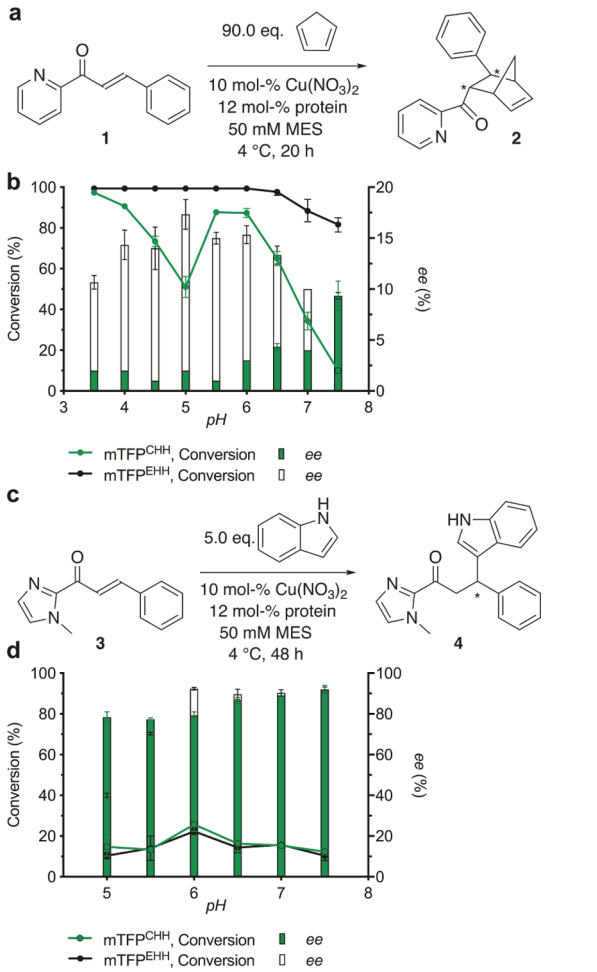

Figure 6. (a) Scheme of catalyzed Diels−Alder reaction with the following conditions: [azachalcone] = 1.0 mM; [cyclopentadiene] = 90 mM; [$Cu(NO_3)_2$] = 0.1 mM; [protein] = 0.12 mM; T = 4 °C; t = 20 h; and reaction volume = 4 mL. Reactions were run at the given pH in 50 mM MES buffer containing 50 mM NaCl. Conversions and ee values were determined by HPLC. (b) Diels−Alderase activity of $mTFP^{CHH}$ and $mTFP^{EHH}$, through various pHs, which revealed appropriate catalytic activity, and up to 17% ee (Table S9). (c) Reaction scheme of catalyzed Friedel−Crafts alkylation with the following conditions: [imidazole] = 1.0 mM; [indole] = 5.0 mM; [$Cu(NO_3)_2$] = 0.1 mM; [protein] = 0.12 mM; T = 4 °C; t = 48 h; and reaction volume = 4 mL. Experiments were run at the given pH in 50 mM MES buffer containing 50 mM NaCl. Conversions and ee values were determined by HPLC. (d) Friedel−Crafts alkylase activity of $mTFP^{CHH}$ and $mTFP^{EHH}$, through various pHs, which resulted in catalytic activity, up to 26% conversion, and up to 92% ee (R enantiomer) (Table S9).

8. DISCUSSION

Since the initial attempt in 1978,[48] numerous strategies were used to produce ArMs. However, only few ArMs were based on the natural amino acid anchoring strategy. In addition, although metal binding motifs have previously been identified within the existing protein scaffolds,[69] the integration of such binding sites within a non-native scaffold, using only natural amino acids, remained unsuccessful. Herein, we present the design and structural and functional characterization of such a novel ArM. Starting from a highly stable fluorescent protein, we engineered a low metal affinity variant, mTFP*, based on selection of surface-exposed metal binding residues, by using

DOI: 10.1021/acscatal.9b02896
ACS Catal. 2019, 9, 11371−11380

FoldX prediction of changes in folding energy for mutants and stability evaluation of highest scoring mutants with MD simulations.

tmFRET titrations revealed that mTFP* possessed only a low, unspecific metal affinity (K_d > 1 mM), whereas the original mTFP1 scaffold had at least two metal binding sites with K_ds of 2.14 ± 0.29 and 268 ± 125 μM. Furthermore, mTFP* tolerates temperatures up to 89 °C, pH values between 2.3 and 12.6, is stable in 10 mM urea at 80 °C, and withstands high organic solvent concentrations. In combination with the crystal structure of mTPF*, we combined computational and experimental approaches to rationally introduce two different metal binding sites into a selected surface pocket ($mTFP^{CHH}$ and $mTFP^{EHH}$). Both $mTFP^{CHH}$ and $mTFP^{EHH}$ revealed high affinities for several metal atoms, with single site K_d^{site} for Cu^{2+} and Zn^{2+} in the μM range. The high enantioselectivities achieved for the Friedel−Crafts alkylation of indole demonstrated that the pocket shape and size of $mTFP^{CHH}$ and $mTFP^{EHH}$ are appropriate to induce sufficient energy differences of the diastereotopic transition states. The initially low stereoselectivity and reaction rates for the Diels−Alder reaction were improved via the modification of the second coordination sphere. Thus, we achieved a catalytic function from a noncatalytic scaffold by rationally introducing amino acid motifs capable of hosting a catalytically active metal atom in a well-defined geometry.

Collectively, we could elucidate that low expression yields, weak protein stability, low recyclability, unspecific cofactor/metal atom ligation, and limited bioavailability can be overcome by developing novel mutants of mTFP*, a derivate from a well-characterized fluorescent protein. We provide a promising fundament on which ArMs can now be advanced based on the natural amino acid anchoring strategy. The absence of artificial cofactors combined with the intrinsic fluorescence of our scaffold markedly facilitates improving or amending implemented catalytic activities (e.g., through directed evolution) and therefore expands the repertoire of ArM templates. Hence, our approach may provide a roadmap for engineering other catalytically active ArMs.

■ ASSOCIATED CONTENT

Supporting Information

The Supporting Information is available free of charge on the ACS Publications website at DOI: 10.1021/acscatal.9b02896.

Supporting Information: Experimental details and data; MD studies for mutants 1−4; molecular biology; characterization of mTFP*; stability investigations; metal binding; metal binding mutants of mTFP*; model of binding pocket; ESI-TOF; altering the second coordination sphere of $mTFP^{CHH}$; selected surface-exposed residues; change in free energy (ΔΔG)*; change in free energy (ΔΔG); list of oligonucleotides; crystallographic parameters; ESI-TOF MS data; spectroscopic characterization; analysis of Cu, Zn, Pd, Ru-$mTFP^{CHH}$, and $mTFP^{EHH}$ by ICP-MS; and catalysis data (PDF)

Supporting Note: Computational details, MD, crystallographic analysis of residual metal binding sites of mTFP*, quantification of metal binding constants via tmFRET, pH dependency of tmFRET, and representative HPLC data for catalysis (PDF)

pH driven structural rearrangement of $mTFP^{CHH}$ (MP4)

■ AUTHOR INFORMATION

Corresponding Authors

*E-mail: stefan.arold@kaust.edu.sa (S.T.A.).
*E-mail: michael.groll@tum.de (M.G.).
*E-mail: jorg.eppinger@kaust.edu.sa (J.E.).

ORCID

Seema Ghorpade: 0000-0001-5576-1390
Stefan T. Arold: 0000-0001-5278-0668
Michael Groll: 0000-0002-1660-340X
Jörg Eppinger: 0000-0001-7886-7059

Present Addresses

⊥L.E.K. Consulting, Brienner Str. 14, 80333 Munich, Germany.
#Division of Digital Science, Thermo Fisher Scientific, Im Steingrund 4, 63303 Dreieich, Germany.
¶Department of Biochemistry, Faculty of Science, Center for Science and Medical Research, University of Jeddah, 80203 Jeddah, Saudi Arabia.

Author Contributions

▽J.F. and D.R. contributed equally to this work.

Funding

The research reported in this publication was supported by King Abdullah University of Science and Technology (KAUST), through the baseline funds and the office of sponsored research under award no. 1974-01, and the TUM/KAUST Joint Doctoral Degree Program.

Notes

The authors declare no competing financial interest.

■ ACKNOWLEDGMENTS

The staff of the Beamline X06SA at the Paul Scherrer Institute, SLS, Villigen, Switzerland, is acknowledged for assistance during data collection. The authors thank S. Abdul Rajjaka for help with the bioinformatic setup.

■ ABBREVIATIONS

ArMs, artificial metalloenzymes
ArM, artificial metalloenzyme
tmFRET, transition metal FRET
MD, molecular dynamics

■ REFERENCES

(1) Lu, Y.; Yeung, N.; Sieracki, N.; Marshall, N. M. Design of Functional Metalloproteins. *Nature* **2009**, *460*, 855−862.
(2) Steinreiber, J.; Ward, T. R. Artificial Metalloenzymes as Selective Catalysts in Aqueous Media. *Coord. Chem. Rev.* **2008**, *252*, 751−766.
(3) Rosati, F.; Roelfes, G. Artificial Metalloenzymes. *ChemCatChem* **2010**, *2*, 916−927.
(4) Deuss, P. J.; den Heeten, R.; Laan, W.; Kamer, P. C. J. Bioinspired Catalyst Design and Artificial Metalloenzymes. *Chemistry* **2011**, *17*, 4680−4698.
(5) Lewis, J. C. Artificial Metalloenzymes and Metallopeptide Catalysts for Organic Synthesis. *ACS Catal.* **2013**, *3*, 2954−2975.
(6) Wallace, S.; Balskus, E. P. Opportunities for Merging Chemical and Biological Synthesis. *Curr. Opin. Biotechnol.* **2014**, *30*, 1−8.
(7) Pordea, A. Metal-binding Promiscuity in Artificial Metalloenzyme Design. *Curr. Opin. Chem. Biol.* **2015**, *25*, 124−132.
(8) Heinisch, T.; Ward, T. R. Latest Developments in Metalloenzyme Design and Repurposing. *Eur. J. Inorg. Chem.* **2015**, 3406−3418.
(9) Bornscheuer, U. T.; Huisman, G. W.; Kazlauskas, R. J.; Lutz, S.; Moore, J. C.; Robins, K. Engineering the Third Wave of Biocatalysis. *Nature* **2012**, *485*, 185−194.

DOI: 10.1021/acscatal.9b02896
ACS Catal. 2019, 9, 11371−11380

(10) Bornscheuer, U. T. The Fourth Wave of Biocatalysis is Approaching. *Philos. Trans. R. Soc., A* **2018**, *376*, 20170063.
(11) Nastri, F.; D'Alonzo, D.; Leone, L.; Zambrano, G.; Pavone, V.; Lombardi, A. Engineering Metalloprotein Functions in Designed and Native Scaffolds. *Trends Biochem. Sci.* **2019**, DOI: 10.1016/j.tibs.2019.06.006.
(12) Landwehr, M.; Hochrein, L.; Otey, C. R.; Kasrayan, A.; Bäckvall, J.-E.; Arnold, F. H. Enantioselective α-Hydroxylation of 2-Arylacetic Acid Derivatives and Buspirone Catalyzed by Engineered Cytochrome P450 BM-3. *J. Am. Chem. Soc.* **2006**, *128*, 6058−6059.
(13) Fasan, R.; Chen, M. M.; Crook, N. C.; Arnold, F. H. Engineered Alkane-Hydroxylating Cytochrome P450BM3 Exhibiting Nativelike Catalytic Properties. *Angew. Chem.* **2007**, *119*, 8566−8570.
(14) Willmann, J. K.; van Bruggen, N.; Dinkelborg, L. M.; Gambhir, S. S. Molecular Imaging in Drug Development. *Nat. Rev. Drug Discovery* **2008**, *7*, 591−607.
(15) Dempsey, J. L.; Winkler, J. R.; Gray, H. B. Proton-Coupled Electron Flow in Protein Redox Machines. *Chem. Rev.* **2010**, *110*, 7024−7039.
(16) Meggers, E. From Conventional to Unusual Enzyme Inhibitor Scaffolds: The Quest for Target Specificity. *Angew. Chem.* **2011**, *50*, 2442−2448.
(17) Razgulin, A.; Ma, N.; Rao, J. Strategies for in vivo Imaging of Enzyme Activity: An Overview and Recent Advances. *Chem. Soc. Rev.* **2011**, *40*, 4186−41216.
(18) Mocny, C. S.; Pecoraro, V. L. De Novo Protein Design as a Methodology for Synthetic Bioinorganic Chemistry. *Acc. Chem. Res.* **2015**, *48*, 2388−2396.
(19) Rudroff, F.; Mihovilovic, M. D.; Gröger, H.; Snajdrova, R.; Iding, H.; Bornscheuer, U. T. Opportunities and Challenges for Combining Chemo- and Biocatalysis. *Nat. Catal.* **2018**, *1*, 12−22.
(20) Romero, P. A.; Arnold, F. H. Exploring Protein Fitness Landscapes by Directed Evolution. *Nat. Rev. Mol. Cell Biol.* **2009**, *10*, 866−876.
(21) Arnold, F. H. Directed Evolution: Bringing New Chemistry to Life. *Angew. Chem., Int. Ed.* **2018**, *57*, 4143−4148.
(22) Zeymer, C.; Hilvert, D. Directed Evolution of Protein Catalysts. *Annu. Rev. Biochem.* **2018**, *87*, 131−157.
(23) Yang, K. K.; Wu, Z.; Arnold, F. H. Machine-Learning-Guided Directed Evolution for Protein Engineering. *Nat. Methods* **2019**, *16*, 687−694.
(24) Markel, U.; Sauer, D. F.; Schiffels, J.; Okuda, J.; Schwaneberg, U. Towards the Evolution of Artificial Metalloenzymes-A Protein Engineer's Perspective. *Angew. Chem., Int. Ed.* **2019**, *58*, 4454−4464.
(25) Xie, J.; Liu, W.; Schultz, P. G. A Genetically Encoded Bidentate, Metal-Binding Amino Acid. *Angew. Chem.* **2007**, *119*, 9399−9402.
(26) Lee, H. S.; Spraggon, G.; Schultz, P. G.; Wang, F. Genetic Incorporation of a Metal-ion Chelating Amino Acid into Proteins as a Biophysical Probe. *J. Am. Chem. Soc.* **2009**, *131*, 2481−2483.
(27) Koebke, K. J.; Pecoraro, V. L. Noncoded Amino Acids in de Novo Metalloprotein Design: Controlling Coordination Number and Catalysis. *Acc. Chem. Res.* **2019**, *52*, 1160−1167.
(28) Mirts, E. N.; Bhagi-Damodaran, A.; Lu, Y. Understanding and Modulating Metalloenzymes with Unnatural Amino Acids, Non-Native Metal Ions, and Non-Native Metallocofactors. *Acc. Chem. Res.* **2019**, *52*, 935−944.
(29) Jing, Q.; Kazlauskas, R. J. Regioselective Hydroformylation of Styrene Using Rhodium-Substituted Carbonic Anhydrase. *ChemCatChem* **2010**, *2*, 953−957.
(30) Key, H. M.; Dydio, P.; Clark, D. S.; Hartwig, J. F. Abiological Catalysis by Artificial Haem Proteins Containing Noble Metals in Place of Iron. *Nature* **2016**, *534*, 534−537.
(31) Levine, H. L.; Nakagawa, Y.; Kaiser, E. T. Flavopapain: Synthesis and Properties of Semi-Synthetic Enzymes. *Biochem. Biophys. Res. Commun.* **1977**, *76*, 64−70.
(32) Davies, R. R.; Distefano, M. D. A Semisynthetic Metalloenzyme Based on a Protein Cavity That Catalyzes the Enantioselective Hydrolysis of Ester and Amide Substrates. *J. Am. Chem. Soc.* **1997**, *119*, 11643−11652.
(33) Reetz, M. T. Directed Evolution of Selective Enzymes and Hybrid Catalysts. *Tetrahedron* **2002**, *58*, 6595−6602.
(34) Ohashi, M.; Koshiyama, T.; Ueno, T.; Yanase, M.; Fujii, H.; Watanabe, Y. Preparation of Artificial Metalloenzymes by Insertion of Chromium(III) Schiff Base Complexes into Apomyoglobin Mutants. *Angew. Chem., Int. Ed.* **2003**, *42*, 1005−1008.
(35) Carey, J. R.; Ma, S. K.; Pfister, T. D.; Garner, D. K.; Kim, H. K.; Abramite, J. A.; Wang, Z.; Guo, Z.; Lu, Y. A Site-Selective Dual Anchoring Strategy for Artificial Metalloprotein Design. *J. Am. Chem. Soc.* **2004**, *126*, 10812−10813.
(36) Panella, L.; Broos, J.; Jin, J.; Fraaije, M. W.; Janssen, D. B.; Jeronimus-Stratingh, M.; Feringa, B. L.; Minnaard, A. J.; de Vries, J. G. Merging Homogeneous Catalysis with Biocatalysis; Papain as Hydrogenation Catalyst. *Chem. Commun.* **2005**, 5656−5658.
(37) Kruithof, C. A.; Casado, M. A.; Guillena, G.; Egmond, M. R.; van der Kerk-van Hoof, A.; Heck, A. J. R.; Klein Gebbink, R. J. M.; van Koten, G. Lipase Active-Site-Directed Anchoring of Organometallics: Metallopincer/Protein Hybrids. *Chemistry* **2005**, *11*, 6869−6877.
(38) Reetz, M. T.; Rentzsch, M.; Pletsch, A.; Maywald, M.; Maiwald, P.; Peyralans, J. J.-P.; Maichele, A.; Fu, Y.; Jiao, N.; Hollmann, F.; Mondière, R.; Taglieber, A. Directed Evolution of Enantioselective Hybrid Catalysts: A Novel Concept in Asymmetric Catalysis. *Tetrahedron* **2007**, *63*, 6404−6414.
(39) Reetz, M. T.; Rentzsch, M.; Pletsch, A.; Taglieber, A.; Hollmann, F.; Mondière, R. J. G.; Dickmann, N.; Höcker, B.; Cerrone, S.; Haeger, M. C.; Sterner, R. A Robust Protein Host for Anchoring Chelating Ligands and Organocatalysts. *ChemBioChem* **2008**, *9*, 552−564.
(40) Dijkstra, H. P.; Sprong, H.; Aerts, B. N. H.; Kruithof, C. A.; Egmond, M. R.; Klein Gebbink, R. J. M. Selective and Diagnostic Labelling of Serine Hydrolases with Reactive Phosphonate Inhibitors. *Org. Biomol. Chem.* **2008**, *6*, 523−531.
(41) Reiner, T.; Jantke, D.; Raba, A.; Marziale, A. N.; Eppinger, J. Side chain functionalized η5-tetramethyl cyclopentadienyl complexes of Rh and Ir with a pendant primary amine group. *J. Organomet. Chem.* **2009**, *694*, 1934−1937.
(42) Deuss, P. J.; Popa, G.; Botting, C. H.; Laan, W.; Kamer, P. C. J. Highly Efficient and Site-Selective Phosphane Modification of Proteins Through Hydrazone Linkage: Development of Artificial Metalloenzymes. *Angew. Chem., Int. Ed.* **2010**, *49*, 5315−5317.
(43) Talbi, B.; Haquette, P.; Martel, A.; de Montigny, F.; Fosse, C.; Cordier, S.; Roisnel, T.; Jaouen, G.; Salmain, M. (η6-Arene) ruthenium(ii) complexes and metallo-papain hybrid as Lewis acid catalysts of Diels-Alder reaction in water. *Dalton Trans.* **2010**, *39*, 5605−5607.
(44) Reiner, T.; Waibel, M.; Marziale, A. N.; Jantke, D.; Kiefer, F. J.; Fässler, T. F.; Eppinger, J. η6-Arene complexes of ruthenium and osmium with pendant donor functionalities. *J. Organomet. Chem.* **2010**, *695*, 2667−2672.
(45) Monnard, F. W.; Heinisch, T.; Nogueira, E. S.; Schirmer, T.; Ward, T. R. Human Carbonic Anhydrase II as a Host for Piano-Stool Complexes Bearing a Sulfonamide Anchor. *Chem. Commun.* **2011**, *47*, 8238−8240.
(46) Reiner, T.; Jantke, D.; Marziale, A. N.; Raba, A.; Eppinger, J. Metal-Conjugated Affinity Labels: A New Concept to Create Enantioselective Artificial Metalloenzymes. *ChemistryOpen* **2013**, *2*, 50−54.
(47) Polizzi, N. F.; Wu, Y.; Lemmin, T.; Maxwell, A. M.; Zhang, S.-Q.; Rawson, J.; Beratan, D. N.; Therien, M. J.; DeGrado, W. F. De novo design of a hyperstable non-natural protein-ligand complex with sub-Å accuracy. *Nat. Chem.* **2017**, *9*, 1157−1164.
(48) Wilson, M. E.; Whitesides, G. M. Conversion of a Protein to a Homogeneous Asymmetric Hydrogenation Catalyst by Site-Specific Modification with a Diphosphinerhodium(I) Moiety. *J. Am. Chem. Soc.* **1978**, *100*, 306−307.
(49) Pierron, J.; Malan, C.; Creus, M.; Gradinaru, J.; Hafner, I.; Ivanova, A.; Sardo, A.; Ward, T. R. Artificial Metalloenzymes for

DOI: 10.1021/acscatal.9b02896
ACS Catal. 2019, 9, 11371−11380

Asymmetric Allylic Alkylation on the Basis of the Biotin-Avidin Technology. *Angew. Chem.* **2008**, *120*, 713−717.
(50) Ward, T. R. Artificial Metalloenzymes Based on the Biotin−Avidin Technology: Enantioselective Catalysis and Beyond. *Acc. Chem. Res.* **2011**, *44*, 47−57.
(51) Mayer, C.; Gillingham, D. G.; Ward, T. R.; Hilvert, D. An Artificial Metalloenzyme for Olefin Metathesis. *Chem. Commun.* **2011**, *47*, 12068−12070.
(52) Lo, C.; Ringenberg, M. R.; Gnandt, D.; Wilson, Y.; Ward, T. R. Artificial Metalloenzymes for Olefin Metathesis Based on the Biotin-(Strept)avidin Technology. *Chem. Commun.* **2011**, *47*, 12065−12067.
(53) Mirts, E. N.; Petrik, I. D.; Hosseinzadeh, P.; Nilges, M. J.; Lu, Y. A Designed Heme-[4Fe-4S] Metalloenzyme Catalyzes Sulfite Reduction like the Native Enzyme. *Science* **2018**, *361*, 1098−1101.
(54) Klein, G.; Humbert, N.; Gradinaru, J.; Ivanova, A.; Gilardoni, F.; Rusbandi, U. E.; Ward, T. R. Tailoring the Active Site of Chemzymes by Using a Chemogenetic-Optimization Procedure: Towards Substrate-Specific Artificial Hydrogenases Based on the Biotin-Avidin Technology. *Angew. Chem.* **2005**, *117*, 7942−7945.
(55) Creus, M.; Pordea, A.; Rossel, T.; Sardo, A.; Letondor, C.; Ivanova, A.; Letrong, I.; Stenkamp, R. E.; Ward, T. R. X-Ray Structure and Designed Evolution of an Artificial Transfer Hydrogenase. *Angew. Chem.* **2008**, *47*, 1400−1404.
(56) Hyster, T. K.; Knorr, L.; Ward, T. R.; Rovis, T. Biotinylated Rh(III) Complexes in Engineered Streptavidin for Accelerated Asymmetric C-H Activation. *Science* **2012**, *338*, 500−503.
(57) Lewis, J. C. Beyond the Second Coordination Sphere: Engineering Dirhodium Artificial Metalloenzymes To Enable Protein Control of Transition Metal Catalysis. *Acc. Chem. Res.* **2019**, *52*, 576−584.
(58) Brodin, J. D.; Medina-Morales, A.; Ni, T.; Salgado, E. N.; Ambroggio, X. I.; Tezcan, F. A. Evolution of Metal Selectivity in Templated Protein Interfaces. *J. Am. Chem. Soc.* **2010**, *132*, 8610−8617.
(59) Yu, F.; Cangelosi, V. M.; Zastrow, M. L.; Tegoni, M.; Plegaria, J. S.; Tebo, A. G.; Mocny, C. S.; Ruckthong, L.; Qayyum, H.; Pecoraro, V. L. Protein Design: Toward Functional Metalloenzymes. *Chem. Rev.* **2014**, *114*, 3495−3578.
(60) Rittle, J.; Field, M. J.; Green, M. T.; Tezcan, F. A. An Efficient, Step-Economical Strategy for the Design of Functional Metalloproteins. *Nat. Chem.* **2019**, *11*, 434−441.
(61) Nanda, V.; Koder, R. L. Designing Artificial Enzymes by Intuition and Computation. *Nat. Chem.* **2010**, *2*, 15−24.
(62) Höhne, M.; Schätzle, S.; Jochens, H.; Robins, K.; Bornscheuer, U. T. Rational Assignment of Key Motifs for Function Guides in silico Enzyme Identification. *Nat. Chem. Biol.* **2010**, *6*, 807−813.
(63) Gonzalez, G.; Hannigan, B.; DeGrado, W. F. A Real-Time All-Atom Structural Search Engine for Proteins. *PLoS Comput. Biol.* **2014**, *10*, No. e1003750.
(64) Hu, X.; Dong, Q.; Yang, J.; Zhang, Y. Recognizing metal and acid radical ion-binding sites by integratingab initiomodeling with template-based transferals. *Bioinformatics* **2016**, *32*, 3260−3269.
(65) Akcapinar, G. B.; Sezerman, O. U. Computational Approaches for de novo Design and Redesign of Metal-Binding Sites on Proteins. *Biosci. Rep.* **2017**, *37*, BSR20160179.
(66) Obexer, R.; Pott, M.; Zeymer, C.; Griffiths, A. D.; Hilvert, D. Efficient Laboratory Evolution of Computationally Designed Enzymes with Low Starting Activities Using Fluorescence-Activated Droplet Sorting. *Protein Eng., Des. Sel.* **2016**, *29*, 355−366.
(67) Bozkurt, E.; Perez, M. A. S.; Hovius, R.; Browning, N. J.; Rothlisberger, U. Genetic Algorithm Based Design and Experimental Characterization of a Highly Thermostable Metalloprotein. *J. Am. Chem. Soc.* **2018**, *140*, 4517−4521.
(68) Ghattas, W.; Dubosclard, V.; Wick, A.; Bendelac, A.; Guillot, R.; Ricoux, R.; Mahy, J.-P. Receptor-Based Artificial Metalloenzymes on Living Human Cells. *J. Am. Chem. Soc.* **2018**, *140*, 8756−8762.
(69) Okamoto, Y.; Kojima, R.; Schwizer, F.; Bartolami, E.; Heinisch, T.; Matile, S.; Fussenegger, M.; Ward, T. R. A Cell-Penetrating Artificial Metalloenzyme Regulates a Gene Switch in a Designer Mammalian Cell. *Nat. Commun.* **2018**, *9*, 1943.
(70) Bunzel, H. A.; Garrabou, X.; Pott, M.; Hilvert, D. Speeding Up Enzyme Discovery and Engineering with Ultrahigh-Throughput Methods. *Curr. Opin. Struct. Biol.* **2018**, *48*, 149−156.
(71) Podtetenieff, J.; Taglieber, A.; Bill, E.; Reijerse, E. J.; Reetz, M. T. An Artificial Metalloenzyme: Creation of a Designed Copper Binding Site in a Thermostable Protein. *Angew. Chem.* **2010**, *49*, 5151−5155.
(72) Jarvo, E. R.; Miller, S. J. Amino Acids and Peptides as Asymmetric Organocatalysts. *Tetrahedron* **2002**, *58*, 2481−2495.
(73) Miller, S. J. In Search of Peptide-Based Catalysts for Asymmetric Organic Synthesis. *Acc. Chem. Res.* **2004**, *37*, 601−610.
(74) Davie, E. A. C.; Mennen, S. M.; Xu, Y.; Miller, S. J. Asymmetric Catalysis Mediated by Synthetic Peptides. *Chem. Rev.* **2007**, *107*, 5759−5812.
(75) Maeda, Y.; Makhlynets, O. V.; Matsui, H.; Korendovych, I. V. Design of Catalytic Peptides and Proteins Through Rational and Combinatorial Approaches. *Annu. Rev. Biomed. Eng.* **2016**, *18*, 311−328.
(76) Studer, S.; Hansen, D. A.; Pianowski, Z. L.; Mittl, P. R. E.; Debon, A.; Guffy, S. L.; Der, B. S.; Kuhlman, B.; Hilvert, D. Evolution of a Highly Active and Enantiospecific Metalloenzyme from Short Peptides. *Science* **2018**, *362*, 1285.
(77) Quintanar, L.; Rivillas-Acevedo, L. Studying Metal Ion−Protein Interactions: Electronic Absorption, Circular Dichroism, and Electron Paramagnetic Resonance. In *Protein-Ligand Interactions: Methods and Applications*; Williams, M. A., Daviter, T., Eds.; Humana Press: Totowa, NJ, 2013, pp 267−297.
(78) Bou-Abdallah, F.; Giffune, T. R. The Thermodynamics of Protein Interactions with Essential First Row Transition Metals. *Biochim. Biophys. Acta* **2016**, *1860*, 879−891.
(79) Wade, H.; Stayrook, S. E.; DeGrado, W. F. The Structure of a Designed Diiron(III) Protein: Implications for Cofactor Stabilization and Catalysis. *Angew. Chem., Int. Ed. Engl.* **2006**, *45*, 4951−4954.
(80) Ruckthong, L.; Zastrow, M. L.; Stuckey, J. A.; Pecoraro, V. L. A Crystallographic Examination of Predisposition versus Preorganization in de Novo Designed Metalloproteins. *J. Am. Chem. Soc.* **2016**, *138*, 11979−11988.
(81) Koebke, K. J.; Ruckthong, L.; Meagher, J. L.; Mathieu, E.; Harland, J.; Deb, A.; Lehnert, N.; Policar, C.; Tard, C.; Penner-Hahn, J. E.; Stuckey, J. A.; Pecoraro, V. L. Clarifying the Copper Coordination Environment in a de Novo Designed Red Copper Protein. *Inorg. Chem.* **2018**, *57*, 12291−12302.
(82) Churchfield, L. A.; Alberstein, R. G.; Williamson, L. M.; Tezcan, F. A. Determining the Structural and Energetic Basis of Allostery in a De Novo Designed Metalloprotein Assembly. *J. Am. Chem. Soc.* **2018**, *140*, 10043−10053.
(83) Yu, Y.; Cui, C.; Liu, X.; Petrik, I. D.; Wang, J.; Lu, Y. A Designed Metalloenzyme Achieving the Catalytic Rate of a Native Enzyme. *J. Am. Chem. Soc.* **2015**, *137*, 11570−11573.
(84) Dydio, P.; Key, H. M.; Nazarenko, A.; Rha, J. Y. E.; Seyedkazemi, V.; Clark, D. S.; Hartwig, J. F. An Artificial Metalloenzyme with the Kinetics of Native Enzymes. *Science* **2016**, *354*, 102.
(85) Klemba, M.; Gardner, K. H.; Marino, S.; Clarke, N. D.; Regan, L. Novel Metal-Binding Proteins by Design. *Nat. Struct. Biol.* **1995**, *2*, 368−373.
(86) Marino, S. F.; Regan, L. Secondary Ligands Enhance Affinity at a Designed Metal-Binding Site. *Chem. Biol.* **1999**, *6*, 649−655.
(87) Petrik, I. D.; Liu, J.; Lu, Y. Metalloenzyme Design and Engineering Through Strategic Modifications of Native Protein Scaffolds. *Curr. Opin. Chem. Biol.* **2014**, *19*, 67−75.
(88) Cunningham, T. F.; Putterman, M. R.; Desai, A.; Horne, W. S.; Saxena, S. The Double-Histidine Cu^{2+}-Binding Motif: A Highly Rigid, Site-Specific Spin Probe for Electron Spin Resonance Distance Measurements. *Angew. Chem.* **2015**, *54*, 6330−6334.
(89) Taraska, J. W.; Puljung, M. C.; Olivier, N. B.; Flynn, G. E.; Zagotta, W. N. Mapping the Structure and Conformational

DOI: 10.1021/acscatal.9b02896
ACS Catal. 2019, 9, 11371−11380

Movements of Proteins with Transition Metal Ion FRET. *Nat. Methods* **2009**, *6*, 532−537.
(90) Taraska, J. W.; Puljung, M. C.; Zagotta, W. N. Short-Distance Probes for Protein Backbone Structure Based on Energy Transfer Between Bimane and Transition Metal Ions. *Proc. Natl. Acad. Sci. U.S.A.* **2009**, *106*, 16227−16232.
(91) Yu, X.; Strub, M.-P.; Barnard, T. J.; Noinaj, N.; Piszczek, G.; Buchanan, S. K.; Taraska, J. W. An Engineered Palette of Metal Ion Quenchable Fluorescent Proteins. *PLoS One* **2014**, *9*, No. e95808.
(92) Bos, J.; Browne, W. R.; Driessen, A. J. M.; Roelfes, G. Supramolecular Assembly of Artificial Metalloenzymes Based on the Dimeric Protein LmrR as Promiscuous Scaffold. *J. Am. Chem. Soc.* **2015**, *137*, 9796−9799.
(93) Drienovská, I.; Rioz-Martínez, A.; Draksharapu, A.; Roelfes, G. Novel Artificial Metalloenzymes by in vivo Incorporation of Metal-Binding Unnatural Amino Acids. *Chem. Sci.* **2015**, *6*, 770−776.
(94) García-Fernández, A.; Megens, R. P.; Villarino, L.; Roelfes, G. DNA-Accelerated Copper Catalysis of Friedel-Crafts Conjugate Addition/Enantioselective Protonation Reactions in Water. *J. Am. Chem. Soc.* **2016**, *138*, 16308−16314.
(95) Bersellini, M.; Roelfes, G. A Metal Ion Regulated Artificial Metalloenzyme. *Dalton Trans.* **2017**, *46*, 4325−4330.
(96) Reetz, M. T.; Jiao, N. Copper-Phthalocyanine Conjugates of Serum Albumins as Enantioselective Catalysts in Diels-Alder Reactions. *Angew. Chem., Int. Ed.* **2006**, *45*, 2416−2419.
(97) Boersma, A. J.; Feringa, B. L.; Roelfes, G. α,β-Unsaturated 2-Acyl Imidazoles as a Practical Class of Dienophiles for the DNA-Based Catalytic Asymmetric Diels−Alder Reaction in Water. *Org. Lett.* **2007**, *9*, 3647−3650.
(98) Coquière, D.; Bos, J.; Beld, J.; Roelfes, G. Enantioselective Artificial Metalloenzymes Based on a Bovine Pancreatic Polypeptide Scaffold. *Angew. Chem., Int. Ed.* **2009**, *48*, 5159−5162.
(99) Rosati, F.; Roelfes, G. A Ligand Structure-Activity Study of DNA-Based Catalytic Asymmetric Hydration and Diels-Alder Reactions. *ChemCatChem* **2011**, *3*, 973−977.
(100) Bos, J.; Fusetti, F.; Driessen, A. J. M.; Roelfes, G. Enantioselective Artificial Metalloenzymes by Creation of a Novel Active Site at the Protein Dimer Interface. *Angew. Chem., Int. Ed.* **2012**, *51*, 7472−7475.
(101) Ward, W. *Green Fluorescent Protein, Properties, Applications and Protocols*; Wiley-Liss, 1998; pp 45−75.
(102) Aouida, M.; Kim, K.; Shaikh, A. R.; Pardo, J. M.; Eppinger, J.; Yun, D.-J.; Bressan, R. A.; Narasimhan, M. L. A Saccharomyces cerevisiae Assay System to Investigate Ligand/AdipoR1 Interactions That Lead to Cellular Signaling. *PLoS One* **2013**, *8*, No. e65454.
(103) Ai, H.-w.; Henderson, J. N.; Remington, S. J.; Campbell, R. E. Directed Evolution of a Monomeric, Bright and Photostable Version of Clavularia cyan Fluorescent Protein: Structural Characterization and Applications in Fluorescence Imaging. *Biochem. J.* **2006**, *400*, 531−540.
(104) Amrein, B.; Schmid, M.; Collet, G.; Cuniasse, P.; Gilardoni, F.; Seebeck, F. P.; Ward, T. R. Identification of Two-Histidines One-Carboxylate Binding Motifs in Proteins Amenable to Facial Coordination to Metals. *Metallomics* **2012**, *4*, 379−388.
(105) Guerois, R.; Nielsen, J. E.; Serrano, L. Predicting Changes in the Stability of Proteins and Protein Complexes: A Study of More Than 1000 Mutations. *J. Mol. Biol.* **2002**, *320*, 369−387.
(106) Van Durme, J.; Delgado, J.; Stricher, F.; Serrano, L.; Schymkowitz, J.; Rousseau, F. A Graphical Interface for the FoldX Forcefield. *Bioinformatics* **2011**, *27*, 1711−1712.
(107) Liu, S.-s.; Wei, X.; Dong, X.; Xu, L.; Liu, J.; Jiang, B. Structural Plasticity of Green Fluorescent Protein to Amino Acid Deletions and Fluorescence Rescue by Folding-Enhancing Mutations. *BMC Biochem.* **2015**, *16*, 17.
(108) McCoy, A. J.; Grosse-Kunstleve, R. W.; Adams, P. D.; Winn, M. D.; Storoni, L. C.; Read, R. J. Phasercrystallographic software. *J. Appl. Crystallogr.* **2007**, *40*, 658−674.
(109) Yu, X.; Wu, X.; Bermejo, G. A.; Brooks, B. R.; Taraska, J. W. Accurate High-Throughput Structure Mapping and Prediction with Transition Metal Ion FRET. *Structure* **2013**, *21*, 9−19.
(110) Ataie, N. J.; Hoang, Q. Q.; Zahniser, M. P. D.; Tu, Y.; Milne, A.; Petsko, G. A.; Ringe, D. Zinc Coordination Geometry and Ligand Binding Affinity: The Structural and Kinetic Analysis of the Second-Shell Serine 228 Residue and the Methionine 180 Residue of the Aminopeptidase fromVibrio proteolyticus. *Biochemistry* **2008**, *47*, 7673−7683.
(111) Shook, R. L.; Borovik, A. S. Role of the Secondary Coordination Sphere in Metal-Mediated Dioxygen Activation. *Inorg. Chem.* **2010**, *49*, 3646−3660.

DOI: 10.1021/acscatal.9b02896
ACS Catal. 2019, 9, 11371−11380